NAR Cancer, 2024, **6**, zcae013
https://doi.org/10.1093/narcan/zcae013
Advance access publication date: 18 March 2024
DNA Damage Sensing and Repair

XPA tumor variant leads to defects in NER that sensitize cells to cisplatin

Alexandra M. Blee[1,2], Kaitlyn S. Gallagher[1,2], Hyun-Suk Kim[3], Mihyun Kim[3,4], Suhas S. Kharat[1,2], Christina R. Troll[5], Areetha D'Souza[1,2], Jiyoung Park[3], P. Drew Neufer[1,2], Orlando D. Schärer[1,3,4] and Walter J. Chazin[1,2,5,*]

[1]Department of Biochemistry, Vanderbilt University, Nashville, TN 37205, USA
[2]Center for Structural Biology, Vanderbilt University, Nashville, TN 37240, USA
[3]Center for Genomic Integrity, Institute for Basic Science, Ulsan 44919, Republic of Korea
[4]Department of Biological Sciences, Ulsan National Institute of Science and Technology, Ulsan 44919, Republic of Korea
[5]Department of Chemistry, Vanderbilt University, Nashville, TN 37240, USA

[*]To whom correspondence should be addressed. Tel: +1 615 936 2210; Fax: +1 615 936 2211; Email: walter.j.chazin@vanderbilt.edu

Abstract

Nucleotide excision repair (NER) reduces efficacy of treatment with platinum (Pt)-based chemotherapy by removing Pt lesions from DNA. Previous study has identified that missense mutation or loss of the NER genes Excision Repair Cross Complementation Group 1 and 2 (*ERCC1* and *ERCC2*) leads to improved patient outcomes after treatment with Pt-based chemotherapies. Although most NER gene alterations found in patient tumors are missense mutations, the impact of mutations in the remaining nearly 20 NER genes is unknown. Towards this goal, we previously developed a machine learning strategy to predict genetic variants in an essential NER protein, Xeroderma Pigmentosum Complementation Group A (XPA), that disrupt repair. In this study, we report in-depth analyses of a subset of the predicted variants, including *in vitro* analyses of purified recombinant protein and cell-based assays to test Pt agent sensitivity in cells and determine mechanisms of NER dysfunction. The most NER deficient variant Y148D had reduced protein stability, weaker DNA binding, disrupted recruitment to damage, and degradation. Our findings demonstrate that tumor mutations in XPA impact cell survival after cisplatin treatment and provide valuable mechanistic insights to improve variant effect prediction. Broadly, these findings suggest XPA tumor variants should be considered when predicting chemotherapy response.

Graphical abstract

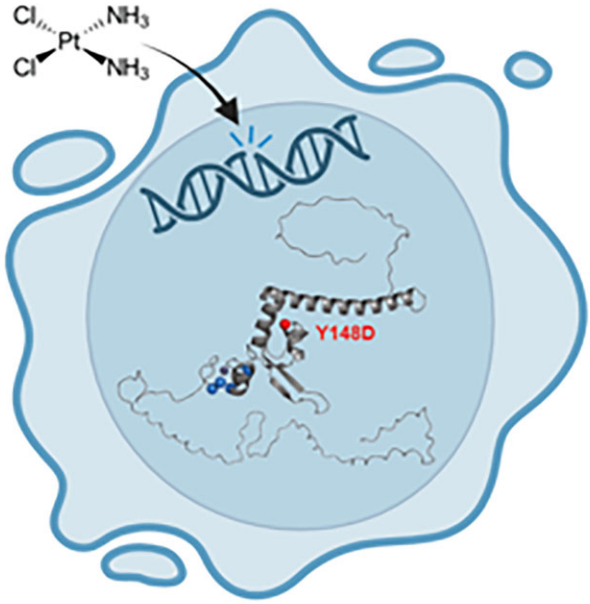

Received: August 11, 2023. **Revised:** January 27, 2024. **Editorial Decision:** February 26, 2024. **Accepted:** February 29, 2024

Introduction

Nucleotide excision repair (NER) protects cells from DNA damage by removing bulky DNA adducts such as those introduced by car exhaust, cigarette smoke, ultraviolet (UV) light, and platinum (Pt)-based chemotherapeutics (1). Germline mutations in genes that reduce NER activity cause the inherited disorder *xeroderma pigmentosum* (XP), hallmarked by extreme sensitivity to solar UV radiation and an over 2000-fold increased incidence of skin cancer (2–4). Reduced NER activity is also correlated with improved tumor response to Pt chemotherapy. Nonrecurrent somatic missense mutations in Excision Repair Cross Complementation Group 2 (*ERCC2*) that lead to defective NER or loss of *ERCC1* has been shown to sensitize tumor cells to cisplatin, leading to improved patient outcomes (5–8). However, the impact of genetic alterations in the remaining NER genes toward Pt therapy remains unknown. Further investigation is motivated by the study of The Cancer Genome Atlas (TCGA) Pan-Cancer Atlas, which revealed that most genetic alterations in NER genes are nonrecurrent nonsynonymous single nucleotide variants of unknown significance (9). The ability to accurately identify deleterious mutations in NER genes from this pool and to determine the mechanisms of reduced repair efficiency that sensitize cells to Pt drugs would better inform clinical decision-making and guide selection of the most successful therapy for individual patients.

Sequence-based genetic variant interpretation represents one strategy to identify mutations that will impact tumor response to therapy, but is severely limited by insufficient benchmarking, lack of data from diverse populations, and absence of functional validation (10). As a robust alternative, we have previously developed a machine learning approach that incorporates functional validation to more accurately predict variants that cause NER defects in cells (11). This prior study focused on tumor variants in the essential NER scaffold protein, Xeroderma Pigmentosum Complementation Group A (XPA). To date, 216 XPA missense variants have been identified in cancer patients sequenced as part of the American Association for Cancer Research (AACR) Project GENIE dataset, the largest public clinicogenomic cancer dataset (183292 sequenced tumors in GENIE Cohort v14.1-public) (12–14). An essential goal of our previous study was to identify variants predicted to sensitize cells to cisplatin from a pool of variants of unknown significance that are otherwise difficult to interpret and lack noticeable features such as recurrent hotspot mutations. While the somatic mutation frequency for XPA in the Project GENIE cohort is only 0.2%, mutations in XPA and defects in NER represented a uniquely well-suited system for these analyses because of the ease in studying XPA at structural, biochemical, and cellular levels with minimal crosstalk between other DNA repair pathways. However, the functional analyses in our previous study were limited to a single DNA repair assay. Here, we report a thorough analysis of a subset of these mutants characterizing their physical properties, NER capacity, and sensitivity to both UV and cisplatin. This investigation is designed to (i) provide evidence to test the hypothesis that NER tumor variants contribute to drug sensitivity in cells, (ii) provide proof-of-concept that our machine learning strategy can predict tumor variants that cause functional repair defects and sensitize cells to cisplatin and (iii) elucidate mechanisms of NER dysfunction.

Five XPA variants from our previous study (F1112C, M113I, D114Y, R130I, Y148D) were of particular interest because they have relatively high confidence predictions of NER-deficiency (11) and are all located in functionally-relevant regions of the globular DNA binding domain (DBD) of XPA. Importantly, across the various cancer genomic databases accessed in the previous study, these five variants occur infrequently and are not recognizable as hotspot mutations that would typically highlight them for further study: F11C occurs once, M113I four times, D114Y once, R130I once and Y148D once across all cancer types. Interestingly, of these five, only M113I, D114Y and Y148D exhibited NER defects in the repair of a UV-damaged reporter using the fluorescence multiplex host cell reactivation (FM-HCR) functional validation assay (11). These discrepancies between the machine learning predictions and repair activity in cells motivated further study. In addition, characterization of these variants provided an opportunity to test repair activity on cisplatin lesions and identify mechanisms of dysfunction associated with each by assessing variant protein structure and stability, DNA binding affinity, interaction with RPA, and recruitment to sites of damage. *In vitro* analyses of purified recombinant variant protein and cell-based assays revealed that our established machine learning strategy can identify XPA variants that disrupt NER and sensitize cells to cisplatin. It also revealed XPA variant protein destabilization, disrupted DNA binding and recruitment to damage, and degradation in cells as key mechanisms of NER dysfunction. The results are discussed in the context of the ongoing efforts to reliably identify tumor variants that will impact response to Pt-based chemotherapeutics.

Materials and methods

Cell lines and cell culture

SV40-transformed human dermal fibroblast XP2OS (XPA-null) cells (15) (RRID:CVCL_F510) were reported in a recent publication. (16) Adenovirus-transformed HEK293FT cells (RRID:CVCL_6911) were gifted from Drs Margaret Axelrod and Justin Balko (Vanderbilt University Medical Center). Cells were cultured in Dulbecco's modified Eagle's medium (DMEM) with high glucose, pyruvate, and GlutaMAX (Thermo Fisher Scientific #10569044) supplemented with 10% qualified One Shot United States Origin Fetal Bovine Serum (FBS) (Thermo Fisher Scientific #A3160502) and 1% Penicillin–Streptomycin (Thermo Fisher Scientific #15140122) at 37°C with 5% CO_2, unless indicated otherwise. Cells were used within three months of thawing and passage number did not exceed 35 for any experiments. Cells were routinely screened and confirmed negative for mycoplasma contamination at least every three months (SouthernBiotech #13100-01).

Plasmids

For recombinant protein expression of both full-length (residues 1–239) and DNA binding domain (residues 98–239) human XPA, cDNA (NM_000380) was cloned into the pBG100 vector (RRID:Addgene_33365) with an N-terminal His_6 tag. Q5 site-directed mutagenesis (New England BioLabs #E05545) was used to generate F112C, M113I, D114Y, R130I or Y148D XPA variants. Mutagenesis primers are

provided in the supplementary information as Supplementary Table S1.

For recombinant protein expression of full-length RPA protein, codon optimized RPA70 was cloned into the pBAD3C vector and RPA14 and 32 were cloned into the pRSFDuet3C vector using restriction enzyme digest. The RPA70 construct contains a N-terminal His-tag, allowing for stoichiometric RPA14 and 32 to pulldown with RPA70 as the complex forms during purification.

For lentiviral transduction, the pMD2.G (RRID:Addgene_12259), psPAX2 (RRID:Addgene_12260) and pWPXL (RRID:Addgene_12257) were used as described. (16) Full-length wild-type (WT), F112C, M113I, D114Y, R130I or Y148D XPA cDNA (NM_000380) was inserted into pWPXL from the previously generated pBG100 (RRID:Addgene_33365) vectors using restriction enzyme digest.

Additional plasmids for recombinant expression of the remaining NER proteins besides XPA and RPA (XPC-RAD23B, (17) XPG, (18) XPF-ERCC1, (19) and TFIIH (20)) have been reported previously.

Antibodies

The following antibodies were used for western blotting: rabbit polyclonal anti-XPA (Abcam ab85914, RRID:AB_1925572) diluted 1:1000, rabbit monoclonal anti-β-tubulin (Cell Signaling Technology #2128S) diluted 1:1000, rabbit monoclonal anti-ubiquitin Lys48-specific (Millipore Sigma 05-1307, RRID:AB_1587578) diluted 1:1000, goat anti-rabbit IgG (H + L) HRP conjugate (Millipore Sigma #AP307P, RRID:AB_92641) diluted 1:5000; and for immunofluorescence: rabbit polyclonal anti-XPA (Abcam ab85914, RRID:AB_1925572) diluted 1:5000, mouse monoclonal anti-(6–4) Photoproducts (6–4PP, Cosmo Bio LTD #CAC-NM-DND-002, RRID:AB_1962842) diluted 1:400, goat anti-rabbit IgG (H + L) Alexa Fluor 488 (Thermo Fisher Scientific #A11008, RRID:AB_143165) diluted 1:1000, and goat anti-mouse IgG (H + L) Alexa Fluor 594 (Thermo Fisher Scientific #A11032, RRID:AB_2534091) diluted 1:1000.

Lentiviral cell line transduction

Lentiviral particles were generated in HEK293FT cells (RRID:CVCL_6911) in 6-well dishes at 70–80% confluency at time of transfection, as described previously (16). Cells were transfected in lentivirus packaging medium containing Opti-MEM supplemented with 5% FBS (Thermo Fisher Scientific #A3160502) and 1 mM sodium pyruvate (Thermo Fisher Scientific #11360070). Transfectant solution included 2.25 μg pMD2.G (RRID:Addgene_12259), 2.25 μg psPAX2 (RRID:Addgene_12260), and 0.75 μg pWPXL (RRID:Addgene_12257) containing WT, F112C, M113I, D114Y, R130I or Y148D XPA, or a mock transfection of XPA-null cells, using 7 μl Lipofectamine 3000 and 6 μl P3000 (Thermo Fisher Scientific #L3000008) in 500 μl total Opti-MEM reduced serum media with GlutaMAX (Thermo Fisher Scientific #51985034) and following manufacturer's instructions for improved lentiviral production. Target XPA-null XP2OS cells (RRID:CVCL_F510) were seeded in 6-well dishes and allowed to reach 50% confluency by time of transduction. Viral particle-containing supernatant was collected 24- and 52-hours post-transfection from HEK293FT cell (RRID:CVCL_6911) plates, 0.2 μm-filtered, and used to transduce XPA-null XP2OS cells (RRID:CVCL_F510). Transduced XP2OS cells (RRID:CVCL_F510) were subsequently cultured as described in the Cell Lines and Cell Culture section.

Western blotting

Cell pellets were harvested on ice and washed with Dulbecco's Phosphate Buffered Saline (DPBS) without calcium chloride or magnesium chloride (Thermo Fisher Scientific #14190-144) before lysing in RIPA lysis buffer (150 mM NaCl, 5 mM EDTA, 50 mM Tris, 1% NP-40, 0.5% sodium deoxycholate, 0.1% SDS, pH 8.0) supplemented with 1× protease inhibitor cocktail (Millipore Sigma #P8340). Lysates were centrifuged to remove cellular debris and protein concentration was measured by DC Protein Concentration Assay (Bio-Rad #5000112) following manufacturer's instructions. Equal amounts of protein (∼50 μg) from cell lysates were denatured in 1× NuPAGE LDS sample buffer (Thermo Fisher Scientific #NP0007) containing 0.1 mM DTT and RIPA buffer, and heated at 95°C for 5 min. Samples were subjected to SDS-polyacrylamide gel electrophoresis (PAGE) in 4–12% NuPAGE Bis-Tris gels (Thermo Fisher Scientific #NP0326BOX) at 100 V for 90 min and wet-transferred to nitrocellulose membranes (Thermo Fisher Scientific #88018) at 30 V for 90 min following manufacturer's instructions. Membranes were briefly stained with Ponceau S (Millipore Sigma #7170) to check for successful transfer. Membranes were blocked in 5% w/v milk in 1× Tris-buffered saline-Tween 20 (TBST, 20 mM Tris, 150 mM NaCl, 0.1% w/v Tween 20, pH 7.6) for 1 h at room temperature and immunoblotted with indicated primary antibodies overnight at 4°C diluted 1:1000 in 5% w/v bovine serum albumin (BSA) in 1× TBST. Membranes were washed 3 times 5 min per wash in 1× TBST at room temperature and incubated with horseradish peroxidase (HRP)-conjugated secondary antibodies diluted 1:5000 in 5% milk w/v in 1× TBST for 1 h at room temperature. Blots were visualized after incubation for 2 min with Pierce ECL Western Blotting Substrate (Thermo Fisher Scientific #32209) following manufacturer's instructions and imaged using a Amersham Imager 600 (GElifesciences/Cytiva). All blot images for analysis were collected prior to detector saturation.

Cell pellets were harvested on ice, washed with 1× DPBS (Thermo Fisher Scientific #14190-144), and lysed in TRIzol (Thermo Fisher Scientific #15596026). RNA was extracted from the TRIzol samples following manufacturer's instructions, using chloroform to separate RNA from DNA and proteins, isopropanol to precipitate the RNA, 75% ethanol to wash the RNA, and nuclease-free water (Thermo Fisher Scientific #10977015) to resuspend the purified RNA pellet. Reverse transcription was performed using the SuperScript IV VILO Master Mix with ezDNase Enzyme reverse transcription kit (Thermo Fisher Scientific #11766050) following manufacturer's instructions including DNase treatment prior to reverse transcription. cDNA was amplified in a CFX96 Touch Real-Time PCR Detection System (Bio-Rad) using Taqman Gene Expression Assay (FAM) probes for *GAPDH* (Thermo Fisher Scientific #4331182, ID: Hs02786624_g1) and *XPA* (Thermo Fisher Scientific #4331182, ID: Hs00902270_m1) following manufacturer's instructions. All reactions for each independent replicate were performed using 100 ng cDNA in triplicate. Relative fold difference in transcript abundance was determined using the $\Delta\Delta C_t$ method (21).

Clonogenic cell survival assay with ultraviolet (UV)-C irradiation

Cells were plated at single cell density in 6 cm dishes with 275 cells per dish and clonogenic cell survival was assayed similarly to as described previously (5,22–24). Cells were allowed to adhere overnight following standard culture conditions, washed with 1× DPBS (Thermo Fisher Scientific #14190-144), and exposed to indicated dose of UV-C (254 nm) radiation before the culture medium was replenished and cells were returned to the temperature and CO_2-controlled incubator. Fourteen days after exposure, cells were fixed with 4% paraformaldehyde (Fisher Scientific #50-980-487) diluted in 1× PBS (137 mM NaCl, 2.7 mM KCl, 10 mM Na_2HPO_4, 1.8 mM KH_2PO_4, pH 7.4) for 15 min at room temperature. The fixative was removed and cells were washed with 1× PBS and then stained with 0.5% crystal violet (Fisher Scientific #C581-25) diluted in water for 60 min. Excess stain was removed and dishes were washed with water. Dishes were imaged using a E-Gel Imager (Thermo Fisher Scientific). Colonies (defined as a minimum of 50 cells) were counted using FIJI. Percent survival was calculated as the percentage of colonies that grew on the treated dishes relative to the untreated dishes at each indicated dose.

Sulforhodamine B colorimetric assay

To test sensitivity to cisplatin, for each independent replicate, cells were plated in triplicate at a density of 4×10^4 cells per well for each planned genotoxin dose, using 96-well plates. Cells were allowed to adhere overnight before treatment with indicated genotoxin following standard culture conditions, incubation for 120 h, fixation, and staining as reported previously. (25–27) At time of treatment, standard culture media was removed and replaced with serum- and antibiotic-free media containing the indicated concentration of genotoxin (zero hour timepoint) and cells were incubated under standard culture conditions for 2 h. After incubation, genotoxin-containing media was removed, wells were washed with 1× DPBS (Thermo Fisher Scientific #14190–144), and standard culture media was replaced. Cells were cultured for an additional 118 h under standard culture conditions. At the 120-hour endpoint, selected to minimize overgrowth of surviving cells post-cisplatin treatment, cells were fixed by removing standard culture media and adding 10% w/v trichloroacetic acid (TCA, Millipore Sigma #91228) and incubation at 4°C for 60 min. Excess 10% TCA was removed, plates were washed by dipping into a basin of gently running water four times, and dried at room temperature. Cells were stained using 0.4% w/v sulforhodamine B sodium salt (Millipore Sigma #S1402) in 1% acetic acid for 30 min at room temperature. Excess stain was removed, each well was washed with 200 µl of 1% acetic acid four times, and plates were dried at room temperature. Protein-bound sulforhodamine B dye was solubilized by adding 100 µl of 10 mM Tris base (Fisher Scientific #BP152-500) to each well and incubation with shaking for 10 min. Absorbance of each well at 490 nm was measured using a BioTek Synergy H1 Hybrid Reader microplate reader. For each independent replicate, a fresh stock of *cis*-Diamineplatinum(II) dichloride (cisplatin, Millipore Sigma, #479306) stock was made by diluting to 2 mM in 0.09% NaCl and incubated for 12 h at room temperature with gentle shaking prior to use, following manufacturer's instructions. To calculate the percent of untreated cell growth, the mean absorbance values were calculated for each triplicate condition and subtracted by the mean absorbance from media-only control wells. The media-subtracted mean absorbances of each genotoxin concentration were divided by those for the corresponding untreated (zero hour) wells and multiplied by 100.

To test proliferation in untreated cells, for each independent replicate, cells were plated in triplicate at a density of 4×10^4 cells per well for each cell line and timepoint, using 96-well plates. Cells were incubated following standard culture conditions for indicated timepoints, fixed and stained as described following the same method as for cisplatin sensitivity.

Bortezomib treatment

For each independent replicate, cells were plated at a density of 1×10^6 cells per well of a 6-well plate and allowed to adhere overnight following standard culture conditions. To inhibit the Ubiquitin Proteasome System (UPS), cells were incubated with 100 nM bortezomib (Fisher Scientific #50-187-1974) for either 0, 2, 4 and 8 h in standard culture media before harvest and processing as described in the Western Blotting section.

XPA expression and purification

Full-length WT or variant XPA protein with a N-terminal His_6 tag in the pBG100 vector was expressed in *Escherichia coli* Rosetta2 pLysS competent cells grown in Terrific Broth medium with 50 µg/ml kanamycin and 10 µM $ZnCl_2$, and cell growth and protein purification were performed similarly to our previous study. (16) Cells were grown to $OD_{600} = 0.6$ at 37°C and then to $OD_{600} = 1.2$ at 18°C, at which point protein expression was induced with 0.5 mM isopropyl β-D-1-thiogalactopyranoside (IPTG) and cells were grown at 18°C for 16 h. Cells were harvested by centrifugation at 6500 rpm for 20 min at 4°C. All subsequent purification steps were performed on ice or at 4°C unless indicated. Cell pellets were resuspended in 10 ml of Lysis Buffer per 1 g of pellet (100 mM Tris pH 8.0, 500 mM NaCl, 20 mM imidazole, 10% glycerol, 5 mM β-mercaptoethanol, 200 µg/ml lysozyme, 10 µl of Roche DNase I recombinant (Millipore Sigma #04536282001), 5 mM magnesium acetate, 1 Roche cOmplete EDTA-free Protease Inhibitor Cocktail tablet (Millipore Sigma #04693132001), 0.5 mM phenylmethylsulfonyl fluoride (PMSF), 1 mM benzamidine) and Dounce homogenized. Cells were further lysed by sonication at 60% amplitude (5 s on/10 s off) for 10 min. Lysate was clarified by centrifugation at 20 000 rpm for 40 min at 4°C and filtration through a 0.45 µm polyvinylidene difluoride (PVDF) syringe filter. Supernatant was incubated with the equivalent of a 5 ml bed of Ni Sepharose High Performance resin (Millipore Sigma #GE17-5268-01) equilibrated with Ni-NTA Buffer A (100 mM Tris pH 8.0, 500 mM NaCl, 20 mM imidazole, 10% glycerol, 5 mM β-mercaptoethanol) for 60 min before passing over a gravity column. Resin was washed with 10 column volumes (CV) of Ni-NTA Buffer A and protein was eluted Ni-NTA Buffer B (100 mM Tris pH 8.0, 500 mM NaCl, 400 mM imidazole, 10% glycerol, 5 mM β-mercaptoethanol). Eluent was incubated with H3C protease for 16 h to cleave the His_6 tag and dialyzed in Pre-Heparin Buffer (20 mM Tris pH 8.0, 300 mM NaCl, 1 mM DTT, 10% glycerol). Dialyzed, cleaved protein was diluted to a final salt concentration of 150 mM NaCl using Dilution Buffer (20 mM Tris pH 8.0, 1 mM DTT, 10% glycerol), applied to a 5 ml HiTrap Heparin HP column

(Cytiva #17040701) equilibrated with Heparin Buffer A (20 mM Tris pH 8.0, 50 mM NaCl, 10% glycerol, 1 mM DTT), washed with 5 CV Heparin Buffer A, washed with a linear gradient of 0–30% Heparin Buffer B (20 mM Tris pH 8.0, 1 M NaCl, 10% glycerol, 1 mM DTT) over 8 CV, and eluted using a linear gradient of 30–70% Heparin Buffer B over 12 CV followed by 5 CV of 100% Heparin Buffer B. XPA protein eluted at approximately 45% Heparin Buffer B. Eluted protein was further purified on a 120 ml HiLoad 16/600 Superdex 75 pg column (Cytiva #28–9893-33) equilibrated with S75 Buffer (50 mM Tris pH 8.0, 150 mM NaCl, 10% glycerol, 1 mM DTT). XPA protein eluted at approximately 65 ml. Protein identity was confirmed by electrospray ionization mass spectrometry and used for experimentation within 24 h after final elution, or aliquoted and flash frozen in liquid nitrogen.

WT or variant XPA DNA binding domain (DBD) protein (residues 98–239) with a N-terminal His_6 tag in the pBG100 vector was expressed in *Escherichia coli* BL21 DE3 competent cells grown in Terrific Broth medium with 50 μg/ml kanamycin and 10 μM $ZnCl_2$. Cell growth and harvest was performed following the same method as for full-length XPA. All subsequent purification steps were performed on ice or at 4°C unless indicated. Cell pellets were resuspended in 10 ml of Ni-NTA Buffer A per 1 g of pellet (20 mM Tris pH 7.5, 500 mM NaCl, 15 mM imidazole, 10% glycerol) plus 1 Roche cOmplete EDTA-free Protease Inhibitor Cocktail tablet (Millipore Sigma #04693132001), 0.5 mM PMSF, and 1 mM benzamidine. Cells were lysed by sonication at 50% amplitude (5 s on/10 s off) for 10 min. Lysate was clarified by centrifugation at 20 000 rpm for 20 min at 4°C and filtration through a 0.45 μm PVDF syringe filter. Supernatant was incubated with the equivalent of a 10 ml bed of Ni Sepharose High Performance resin (Millipore Sigma #GE17-5268-01) equilibrated with Ni-NTA Buffer A (100 mM Tris pH 8.0, 500 mM NaCl, 20 mM imidazole, 10% glycerol, 5 mM β-mercaptoethanol) for 60 min before passing over a gravity column. Resin was washed with 10 column volumes (CV) of Ni-NTA Buffer A and protein was eluted Ni-NTA Buffer B (20 mM Tris pH 7.5, 500 mM NaCl, 400 mM imidazole, 10% glycerol). Eluent was diluted to a final salt concentration of 150 mM NaCl using Dilution Buffer (20 mM Tris pH 7.5, 1 mM DTT, 10% glycerol) and incubated with H3C protease for 3 h to cleave the His_6 tag. Diluted, cleaved protein was applied to a 5 ml HiTrap Heparin HP column (Cytiva #17040701) equilibrated with Heparin Buffer A (20 mM Tris pH 7.5, 150 mM NaCl, 10% glycerol, 1 mM DTT), washed with 8 CV Heparin Buffer A, and eluted using a linear gradient of 0–100% Heparin Buffer B (20 mM Tris pH 8.0, 1 M NaCl, 10% glycerol, 1 mM DTT) over 12 CV followed by 3 CV of 100% Heparin Buffer B. XPA protein eluted at approximately 50% Heparin Buffer B. Eluted protein was further purified on a 24 ml Superdex Increase 75 10/300 column (Cytiva #29-1487-21) equilibrated with S75 Buffer (20 mM Tris pH 7.5, 150 mM NaCl, 10% glycerol, 1 mM DTT). XPA protein eluted at approximately 11 ml. Protein identity was confirmed by electrospray ionization mass spectrometry and used for experimentation within 24 h after final elution, or aliquoted and flash frozen in liquid nitrogen.

For both the full-length and DBD constructs of the Y148D XPA variant, refolding was necessary to obtain yields of soluble protein. The expression and purification methods were modified as follows. Cells were grown in Luria-Bertani (LB) broth medium with 50 μg/ml kanamycin and 10 μM $ZnCl_2$. Cells were grown to OD_{600} = 0.6 at 37°C and then to OD_{600} = 1.2 at 18°C, at which point protein expression was induced with 0.25 mM IPTG and cells were grown at 18°C for 16 h. Cells were harvested by centrifugation at 6500 rpm for 20 min at 4°C. All subsequent purification steps were performed on ice or at 4°C unless indicated. Cell pellets were resuspended and lysed following the same method as described for WT and other variant XPA proteins. Lysate was clarified by centrifugation at 20 000 rpm for 20 min at 4°C. Insoluble Y148D XPA protein present in the pellet after centrifugation was subjected to a second round of resuspension, lysis, and centrifugation as described. Taking the pelleted sample, resuspend in 10 ml of Ni-NTA Buffer A with 4 M guanidinium hydrochloride (GuHCl) per original 1 g of original pellet. Cells were lysed by sonication at 50% amplitude (5 s on/10 s off) for 10 min. Lysate was clarified by centrifugation at 20 000 rpm for 20 min at 4°C. The denatured protein in the supernatant was collected and four serial dialysis steps into Ni-NTA Buffer A were performed to remove the GuHCl from the sample. Dialyzed sample was filtered through a 0.45 μm PVDF syringe filter. Purification continued beginning with Ni Sepharose High Performance resin as described for WT and other XPA variant proteins.

RPA expression and purification

Full-length RPA protein (RPA70, RPA32 and RPA14 constructs) was expressed in Rosetta2 pLysS competent cells grown in Terrific Broth medium with 50 μg/ml kanamycin and 100 μg/ml ampicillin. Cells were grown to OD_{600} = 0.8 at 37°C and then to OD_{600} = 1.1 at 18°C, at which point protein expression was induced with 1 mM IPTG and 2 g/l of L-Arabinose and cells were grown at 18°C for 16 h. Cells were harvested by centrifugation at 6500 rpm for 20 min at 4°C. All subsequent purification steps were performed on ice or at 4°C unless indicated. Cell pellets were resuspended in 5 ml of Lysis Buffer per 1 g of pellet (20 mM HEPES pH 7.5, 500 mM NaCl, 5 mM β-mercaptoethanol, 10 μM $ZnCl_2$, 10 mM imidazole, 2 Roche cOmplete EDTA-free Protease Inhibitor Cocktail tablets (Millipore Sigma #04693132001). Cells were further lysed by sonication at 60% amplitude (5 s on/5 s off) for 5 min. Lysate was clarified by centrifugation at 20 000 rpm for 40 min at 4°C and filtration through a 0.45 μm PVDF syringe filter. Supernatant was applied to a 5 ml HisTrap HP column (Cytiva #17524801) equilibrated with Ni-NTA Buffer A (20 mM HEPES pH 7.5, 500 mM NaCl, 5 mM β-mercaptoethanol, 10 μM $ZnCl_2$, 10 mM imidazole). Column was washed with a linear gradient of 0–10% Ni-NTA Buffer B (20 mM HEPES pH 7.5, 500 mM NaCl, 5 mM β-mercaptoethanol, 10 μM $ZnCl_2$, 300 mM imidazole) over 11 CV, and eluted using a linear gradient of 60–100% Ni-NTA Buffer B over 6 CV. RPA protein eluted at approximately 70–80% Ni-NTA Buffer B. Eluent was incubated with H3C protease for 1 hour at room temperature to cleave the His_6 tag and dialyzed in Pre-Heparin Buffer (20 mM HEPES pH 7.5, 300 mM NaCl, 5 mM β-mercaptoethanol, 10 μM $ZnCl_2$, 10% glycerol) for 3 h at 4°C. Dialyzed, cleaved protein was diluted to a final salt concentration of 150 mM NaCl using Dilution Buffer (20 mM HEPES pH 7.5, 5 mM β-mercaptoethanol, 10 μM $ZnCl_2$, 10% glycerol). Sample was applied to a 5 ml HiTrap Heparin HP column (Cytiva #17040701) equilibrated with Heparin Buffer A (20 mM HEPES pH 7.5, 50 mM NaCl, 5 mM β-mercaptoethanol,

10 μM $ZnCl_2$, 10% glycerol), washed with a linear gradient of 0–15% Heparin Buffer B (20 mM HEPES pH 7.5, 1 M NaCl, 5 mM β-mercaptoethanol, 10 μM $ZnCl_2$, 10% glycerol) over 6 CV, 15% Heparin Buffer B over 8 CV, and eluted using a linear gradient of 15–50% Heparin Buffer B over 10 CV, followed by 100% Heparin Buffer B over 6 CV. RPA protein eluted at approximately 25% Heparin Buffer B. Eluted protein was further purified on a 24 ml Superdex 200 Increase 10/300 GL column (Cytiva #28-9909-44) equilibrated with S200 Buffer (20 mM Tris pH 7.5, 200 mM NaCl). RPA protein eluted at approximately 13 ml. Protein identity was confirmed by electrospray ionization mass spectrometry and used for experimentation within 24 h after final elution, or aliquoted and flash frozen in liquid nitrogen.

In vitro NER activity assay with purified proteins

A plasmid substrate containing a site-specific 1,3-GTG cisplatin intrastrand crosslink was generated from p98 plasmids employing gapped-vector technology using a purified 24-mer of the platinated oligonucleotide (5′-pTCTTCTTCT**GTG**CACTCTTCTTCT). (28) The plasmid containing and the essential purified, recombinant NER proteins except XPA required to reconstitute dual-incision activity *in vitro* was incubated with either wild-type or variant XPA as described previously. (16) For each reaction, 5 nM XPC-RAD23B, 40 nM RPA, 27 nM XPG, 13.3 nM XPF-ERCC1 and 10 nM TFIIH was complemented with 20 nM WT or variant XPA. All proteins were > 95% pure. Full-length XPA and RPA were produced as described in Materials and Methods, and all remaining proteins were produced as previously described: XPC-RAD23B (17), XPG (18), XPF-ERCC1 (19) and TFIIH (20). Incision reactions were conducted in repair buffer (45 mM HEPES-KOH pH 7.8, 5 mM $MgCl_2$, 0.3 mM EDTA, 40 mM phosphocreatine di-Tris salt, 2 mM ATP, 1 mM DTT, 2.5 μg/μl BSA, 0.05 μg/μl creatine phosphokinase, and 70 mM NaCl) at 30°C for indicated times. A 3′-phophorylated oligonucleotide (0.5 μl of 1 μM solution) was added for product labeling and the mixture heated at 95°C for 5 min. The mixture was cooled to room temperature over 15 min. 1.2 μl of a Sequenase/[α^{32}P]-dCTP mix (0.25 units of Sequenase and 2.5 μCi of [α32P]-dCTP per reaction) was added and incubated at 37°C for 3 min. Then 1.2 μl of dNTP mix (100 μM of each dATP, dTTP, dGTP; 50 μM dCTP) was added to mixture and incubated for another 12 min. The reactions were stopped by adding 12 μl of loading dye (80% formamide/10 mM EDTA) and heating at 95°C for 5 min. 6 μl of sample was loaded on 14% sequencing gel (7 M urea, 0.5× TBE) and electrophoresed at 45 W for 2.5 h. The reaction products were visualized using a PhosphorImager (Amersham Typhoon RGB, GE Healthcare Bio-Sciences). Two independent repetitions were performed. The NER products were quantified by ImageQuant TL and normalized to the amount of NER product formed with WT-XPA at 45 min.

Circular dichroism (CD) spectroscopy

CD spectra were recorded and thermal denaturation monitored by CD for indicated XPA DBD proteins similarly as described previously, (29–31) using a Jasco J-810 spectropolarimeter and a quartz cuvette. Protein samples were used within 24 h after purification or thawed from flash frozen aliquots, exchanged into 150 mM KH_2PO_4 buffer at pH 7.5, and 0.2 μm filtered. The far-UV spectrum was measured for 0.1 mg/ml protein samples from 260 to 190 nm in increments of 0.5 nm at a rate of 50 nm/min with a response time of 2 s and a bandwidth of 1 nm. For each independent experiment, three spectra were averaged and smoothed for each protein and a buffer blank spectrum was subtracted.

For thermal denaturation, CD was monitored for 0.5 mg/ml protein samples every 1.0°C at 222 nm as the temperature was increased from 20 to 80°C for 90 min, and the first derivative curve was generated for the resulting buffer blank-subtracted curve. The mean apparent T_m was determined by taking the average of the temperatures corresponding to the maximum values from each first derivative curve for three independent denaturation experiments.

Microscale thermophoresis (MST)

MST to measure DNA binding affinity was performed as described previously (16,32). DNA binding affinity of indicated XPA DBD proteins for a 5′ 6-FAM-labeled 8 nucleotide (nt) hairpin substrate with a 4 nt overhang (5′-6-FAM-TTTTGCGGCCGCTTTTGCGGCCGC-3′) was measured using a Monolith NT.115 (NanoTemper Technologies). DNA substrate was prepared for use by diluting to working concentration of 440 nM in Substrate Buffer (6 mM Tris pH 7.5, 60 mM KCl, 0.2 mM $MgCl_2$), heating at 95°C for 5 min, and cooling on ice. Indicated XPA proteins were used within 24 h after purification or thawed from flash frozen aliquots and filtered using 0.2 mm wwPTFE Pall Nanosep centrifugal filters (Pall #ODPTFE02C35). Protein samples were buffer exchanged into XPA MST Buffer (50 mM Tris–HCl pH 7.8, 150 mM NaCl, 10 mM $MgCl_2$, 0.05% Tween-20, 1 mM DTT) and diluted into 16 concentrations ranging from 0.1 to 50 μM on ice. Immediately prior to measuring affinity, DNA substrate was added to each protein sample to a final concentration of 40 nM. All measurements for each independent replicate were carried out with four technical replicates for each protein concentration. Measurements were taken at room temperature using standard capillaries (NanoTemper Technologies #MO-K022) with MST power set to low and laser excitation power set to 20%. Fraction of substrate bound at each XPA concentration was reported using values output by the MO. Affinity-Analysis software (NanoTemper Technologies). Y148D XPA DBD could not be concentrated to the final 50 μM datapoint due to limited solubility.

Isothermal titration calorimetry (ITC)

ITC was performed with purified full-length XPA and RPA protein samples as described previously (16). Protein samples were used within 24 h after purification or thawed from flash frozen aliquots and dialyzed into ITC Buffer (20 mM Tris pH 8.0, 150 mM NaCl, 3% glycerol, 0.5 mM tris(2-carboxyethyl)phosphine (TCEP)). All buffers and protein samples were 0.2 μm filtered and degassed prior to beginning. Titrations were performed at 25°C with 125 rpm stirring using a Affinity ITC instrument (TA Instruments), and included an initial injection of 0.5 μl of 115 μM XPA into the sample cell containing 20 μM RPA, followed by an additional 47 injections of 3 μl each. Injections were spaced over 200–250 s intervals. Data were analyzed using NanoAnalyze (TA Instruments) and the thermodynamic parameters and binding affinities were calculated using the average of two or three titrations fit to an independent binding model.

Local UV irradiation assay

Local UV irradiation was performed similar to our previous protocol (16,33). Cells were plated onto glass coverslips (Millipore Sigma #CLS285022) coated with 1 μg/ml fibronectin (Millipore Sigma #F4759) at a density of 5.0×10^5 cells per well of a 6-well plate and incubated overnight following standard culture conditions. Adherent cells were washed once with 1× DPBS (Thermo Fisher Scientific #14190-144) and the coverslip was removed and placed cell-side up onto a clean 10 cm dish covered with parafilm for UV irradiation. A polycarbonate isopore membrane filter with 5 μm pores (Millipore Sigma #TMTP04700) was pre-soaked in 1× DPBS and placed directly on top of the coverslip, and cells were irradiated with 120 J/m^2 of UV-C. Post-irradiation, the membrane filter was gently removed and the coverslip was returned to a 6-well plate with fresh culture media and incubated following standard culture conditions for 30 min. Coverslips were washed once with cold 1× PBS and cells permeabilized with Hypotonic Lysis Buffer (10 mM Tris–HCl pH 8.0, 2.5 mM $MgCl_2$, 10 mM β-glycerophosphate, 0.2 mM PMSF, 0.1 mM Na_3VO_4, 0.1% Igepal) for 8 min on ice. Coverslips were washed with Hypotonic Lysis Buffer without Igepal for 4 min at room temperature. Cells were fixed with 4% paraformaldehyde (Fisher Scientific #50–980-487) freshly diluted in 1× PBS (137 mM NaCl, 2.7 mM KCl, 10 mM Na_2HPO_4, 1.8 mM KH_2PO_4, pH 7.4) for 15 min at room temperature with gentle shaking. Permeabilized, fixed cells were incubated with 0.07 M NaOH in 1× PBS for 3 min at room temperature to denature DNA and then washed 5 times for 3 min each time with 1× PBS. Cellular localization for proteins of interest was then visualized after performing the described immunofluorescence protocol and imaging of coverslips using a Zeiss fluorescence microscope and X-Cite fluorescence lamp. The percent cells with co-localized foci was determined for each independent replicate by quantifying the number of cells with overlapping XPA and 6–4PP foci out of 100 cells with 6–4PP foci using FIJI.

Immunofluorescence

For immunofluorescence, coverslips were blocked in 1% bovine serum albumin (BSA, Millipore Sigma #A2153) with 10% normal goat serum (Vector Laboratories #S-1000-20) in 1× PBS for 1 h at room temperature. Coverslips were incubated with indicated primary antibodies in 1× PBST (1× PBS with 0.1% Tween-20) with 1% BSA and 2% normal goat serum for 2 h at room temperature in humid conditions. Primary antibody solution was removed and coverslips were washed 3 times for 5 min each with 1× PBST. Coverslips were incubated with indicated secondary antibodies in 1× PBST with 1% BSA and 2% normal goat serum for 1 h at room temperature in dark and humid conditions. Secondary antibody solution was removed and coverslips were washed 2 times for 5 min each with 1× PBST. Coverslips were washed for 5 min in 1× PBS with 300 nM 4′-6′-damino-2-phenylindole (DAPI, dihydrochloride, Millipore Sigma #D9542). Coverslips were briefly rinsed twice with 1× PBS, mounted onto microscope slides with ProLong Diamond Antifade Mountant (Thermo Fisher Scientific #P36970), and sealed with nail polish.

Slot-blot assay

Cells were irradiated with 10 J/m^2 of UV-C and collected after UV exposure for different time points (0, 2, 4, 6, 8 h). Genomic DNA from harvested cells was isolated using the QIAamp DNA mini kit (Qiagen). 400 ng of genomic DNA was denatured by heating at 95°C for 10 min in 7.8 mM EDTA. DNA was neutralized by adding an equal volume of 2 M ammonium acetate (pH 7.0) and vacuum-transferred to a prewashed nitrocellulose membrane using a BioDot SF microfiltration apparatus (Bio-Rad). Each well was washed 2 times with 2× SSC buffer. The membrane was removed from the apparatus, rinsed twice with 2× SSC, air dried, hybridized at 80°C for 2 h, and blocked with 5% skim milk in PBS for 30 min. For lesion detection, the membrane was incubated with mouse monoclonal anti-(6–4) Photoproducts (6–4PP, Cosmo Bio LTD #CAC-NM-DND-002, RRID:AB_1962842) antibody diluted 1:2000 at 4°C overnight and then incubated with goat anti-mouse IgG (H + L) HRP conjugate (Millipore Sigma #AP308P, RRID:AB_92635) antibody diluted 1:5000 for 1 h at room temperature. The blot was visualized with ECL system (Thermo Fisher Scientific) and the total amount of DNA loaded on the membrane was visualized with SYBR-gold staining (Thermo Fisher Scientific).

Statistical analyses

Statistical analyses were performed in GraphPad Prism (RRID:SCR_002798). Details on sample sizes, tests used, error bars and statistical significance values are provided in the figures and figure legends.

Results

Cells stably expressing predicted NER-deficient tumor variants have increased sensitivity to UV and cisplatin

All five XPA tumor variants selected for this analysis were predicted to have a high probability of being NER-deficient, P(NER-deficient), values of F112C = 0.962, M113I = 0.75, D114Y = 0.978, R130I = 0.993, Y148D = 0.849 (11), and thus also predicted to sensitize cells to UV light and Pt-based chemotherapeutics. Moreover, each of the mutations are located in functionally relevant regions of the protein: F112, M113 and D114 are at an essential XPA-RPA interaction interface that is required for NER activity (16,32), R130 contacts the DNA substrate (32), and Y148 is a buried hydrophobic residue within the globular core of the XPA DNA binding domain (DBD) (34–37).

The five XPA variants were stably expressed in SV40-transformed human dermal fibroblast XP2OS cells, which lack expression of wild-type (WT) XPA protein (15). Stable, lentivirus-mediated expression of either WT or variant XPA was confirmed by western blot (Supplementary Figure S1A). As expected, the overexpression of XPA in these cells did not alter cell proliferation in any of the cell lines (Supplementary Figure S1B). Although the majority of variants were expressed at levels similar to WT protein, there was a ten-fold reduction in Y148D XPA protein compared to WT protein. Control experiments showed this was not due to a difference in lentiviral transduction efficiency or issues with mRNA expression (Supplementary Figure S1C). Protein degradation via the Ubiquitin Proteasome System (UPS) is a common mechanism for regulating protein levels and a means to rid the cell of misfolded or destabilized proteins. (38,39) To test whether the Y148D mutation leads to more ready degradation via the UPS, cells stably expressing WT or Y148D XPA as well

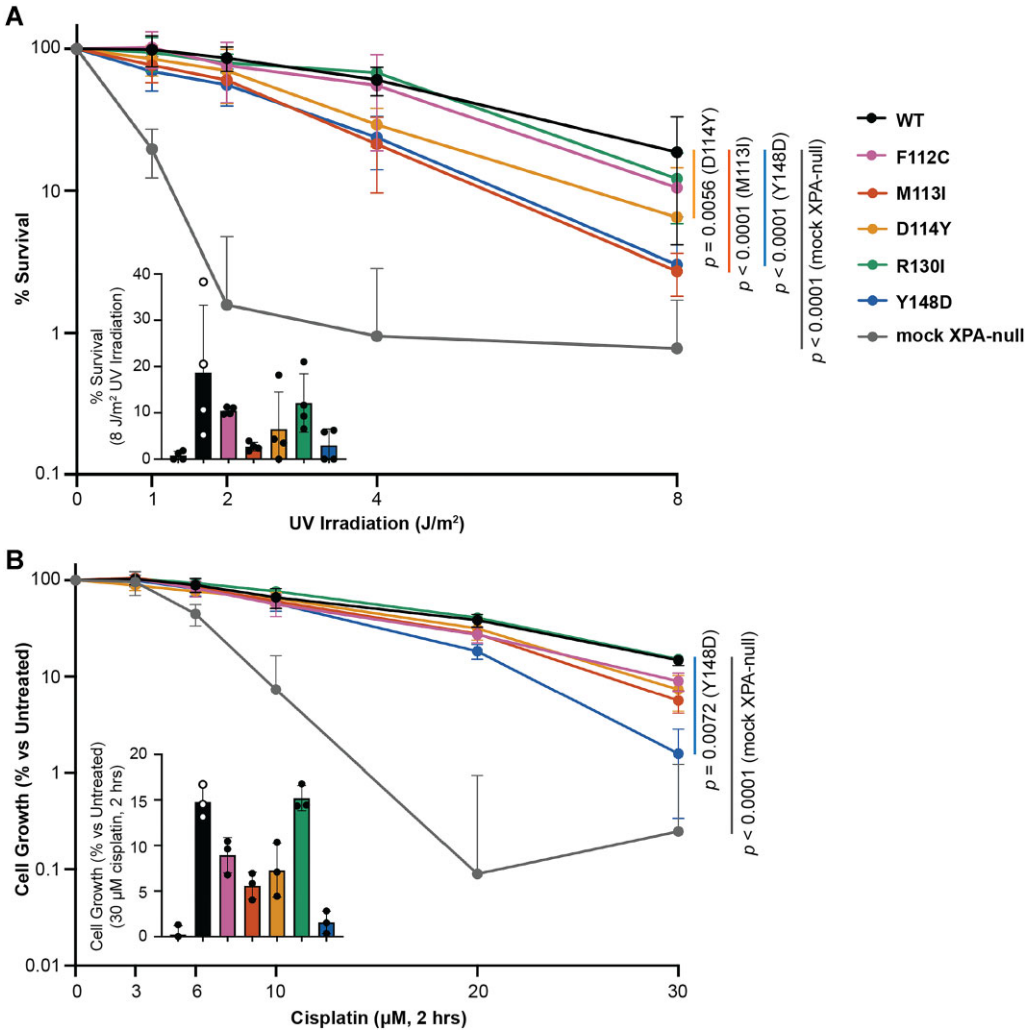

Figure 1. Cells stably expressing NER-deficient XPA tumor variants have increased sensitivity to UV and cisplatin. (**A**) Clonogenic cell survival assay in stable XP2OS cell lines after exposure to UV at indicated doses and growth for 14 days ($n = 4$). Colonies were stained with 0.5% crystal violet and those greater than approximately 50 cells were counted using Fiji. Percent survival was determined for each cell line relative to untreated. IC_{50} values [95% confidence intervals (CI)] determined using lines of best fit from nonlinear regression analysis in GraphPad Prism ([inhibitor] versus response–variable slope (four parameters equation): 0.6 J/m^2 [0.2–0.8 J/m^2] (mock XPA-null), 5 J/m^2 [4–6 J/m^2] (WT), 4 J/m^2 [3–5 J/m^2] (F112C), 2 J/m^2 [2–3 J/m^2] (M113I), 3 J/m^2 [2–4 J/m^2] (D114Y), 5 J/m^2 [4–6 J/m^2] (R130I) and 2 J/m^2 [2–3 J/m^2] (Y148D). EC50 shift, X is concentration equation in GraphPad Prism used to compare the IC_{50} from each line of best fit to that of the WT control, indicating comparisons to WT with $P < 0.05$. Inset showing mean percent survival for each cell line at 8 J/m^2 UV irradiation. Additional P values for EC50 shift, X is concentration equation in GraphPad Prism used to compare the IC_{50} from each line of best fit to that of the mock XPA-null control: F112C $P < 0.0001$; M113I $P < 0.0001$; D114Y $P < 0.0001$; R130I $P < 0.0001$; Y148D $P < 0.0001$. (**B**) SRB assay in stable XP2OS cell lines after exposure to cisplatin for 2 h at indicated doses and growth for 5 days ($n = 3$). Cells were stained with 0.4% SRB and absorbance at 490 nm measured. Percent untreated cell growth was determined for each cell line relative to untreated. IC_{50} values [95% CI] determined using lines of best fit from nonlinear regression analysis in GraphPad Prism ([inhibitor] versus response–variable slope (four parameters equation): 6 μM [5–7 μM] (mock XPA-null), 15 μM [12–18 μM] (WT), 12 μM [11–15 μM] (F112C), 13 μM [11–15 μM] (M113I), 13 μM [11–16 μM] (D114Y), 17 μM [15–20 μM] (R130I) and 11 μM [10–14 μM] (Y148D). EC50 shift, X is concentration equation used to compare the IC_{50} of each line of best fit to that of the WT control, indicating comparisons to WT with $P < 0.05$. Legend in panel (A). Inset showing mean cell growth for each cell line at 30 μM cisplatin. Additional P values for EC50 shift, X is concentration equation in GraphPad Prism used to compare the IC_{50} from each line of best fit to that of the mock XPA-null control: F112C $P < 0.0001$; M113I $P < 0.0001$; D114Y $P < 0.0001$; R130I $P < 0.0001$; Y148D $P < 0.0001$.

as mock XPA-null cells were treated with the UPS inhibitor bortezomib (40,41) and levels of XPA were assessed by Western blot. UPS inhibition led to a partial rescue of Y148D protein levels (Supplementary Figure S1D–E). These data indicate that the lower level of Y148D is mediated at least in part by degradation by the UPS, and that this must be accounted for in our subsequent analyses.

In order to determine whether these XPA variants cause NER defects in the context of damage to native chromatin, cells were first tested for hypersensitivity to UV light using a clonogenic cell survival assay. Compared to cells expressing WT XPA, cells expressing F112C or R130I XPA did not exhibit increased sensitivity to UV. In contrast, cells expressing M113I, D114Y, and Y148D XPA showed a statistically significant increase in sensitivity to UV irradiation (IC_{50} [95% confidence interval (CI)] = 5 J/m^2 [4–6 J/m^2], 2 J/m^2 [2–3 J/m^2], 3 J/m^2 [2–4 J/m^2], 2 J/m^2 [2–3 J/m^2], for WT, M113I, D114Y and Y148D, respectively) (Figure 1A, Supplementary Figure S2). Reassuringly, this data agreed with our previous findings using a UV-damaged reporter plas-

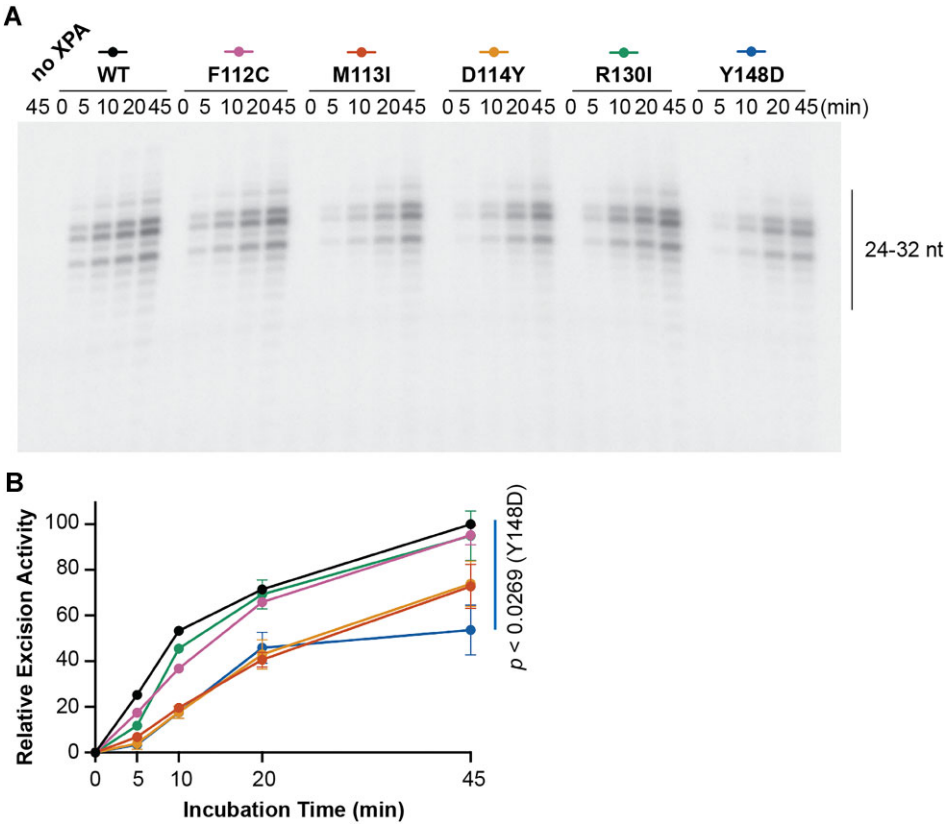

Figure 2. XPA tumor variants are defective in dual-incision of a NER-specific cisplatin lesion *in vitro*. (**A**) *In vitro* NER activity of purified NER proteins RPA (40 nM), XPC-RAD23B (5 nM), XPG (27 nM), XPF-ERCC1 (13 nM) and TFIIH (10 nM) complemented with WT or variant XPA (20 nM) on a plasmid containing a 1,3-GTG cisplatin intrastrand crosslink ($n = 2$). Gel shows excision products. (**B**) Excised band intensities for the reconstituted complexes containing each different XPA protein, as indicated by the legend in (A). Relative excision activity was determined as percentage of the WT XPA excision activity at 45 min. Mean relative excision activity values at 45 min were compared for each variant to WT using two-tailed unpaired *t*-tests, and *P*-values for statistically significant relative excision activity compared to WT ($P < 0.05$) are indicated.

mid in a host-cell reactivation assay (FM-HCR), (11) which showed these variants have reduced capacity for the repair of UV lesions.

A similar analysis of cisplatin hypersensitivity of two sets of independently generated stable cell lines was performed using a sulforhodamine B assay. These experiments revealed that only cells expressing the Y148D variant XPA had a statistically significant increase in cisplatin sensitivity compared to WT XPA-expressing cells: cell line set 1 (IC_{50} [95% CI] = 11 μM [10–14 μM] for Y148D XPA versus 15 μM [12–18 μM] for WT XPA) (Figure 1B), and cell line set 2 (IC_{50} [95% CI] = 14 μM [11–15 μM] for Y148D XPA versus 18 μM [15–20 μM] for WT XPA) (Supplementary Figure S3A–B). Some cisplatin lesions can be repaired by non-NER pathways including double-strand break (DSB) repair and interstrand crosslink (ICL) repair, (42) which may explain the differences observed between repair of UV and cisplatin lesions in the cellular assays. Regardless, our results suggest that expression of the Y148D XPA tumor variant in cells leads to decreased efficiency in the repair of both UV and cisplatin lesions.

XPA tumor variants are defective in dual-incision of a NER-specific cisplatin lesion *in vitro*

To further address the difference between the UV and cisplatin sensitivity and obtain deeper insights into the functionality of XPA tumor variants, an *in vitro* repair assay with a NER-specific 1,3-GTG cisplatin intrastrand crosslink lesion (43–46) was performed. Purified recombinant NER proteins RPA, XPC-RAD23B, XPG, XPF-ERCC1 and TFIIH were complemented with equal concentrations of WT or variant XPA protein and the appearance of NER excision products was monitored in a time-dependent manner. Importantly, as opposed to the assays performed in stable cell lines, this *in vitro* reconstitution also allowed direct comparison of the effect of different variants on NER that was independent of native cellular concentration. This was particularly important for the comparative analysis of Y148D. Consistent with the decreased levels of Y148D observed in cells (Supplementary Figures S1A and S3A), we note that the recombinant protein was expressed primarily in the insoluble fraction and required unique approaches to obtain sufficient quantities of protein for use in this assay.

Reconstitution of the NER reaction *in vitro* without XPA did not lead to excision products for the damaged substrate, whereas addition of WT, F112C or R130I XPA led to robust accumulation of excision products over time (Figure 2A, B and Supplementary Figure S4). These results agreed with the lack of hypersensitivity to UV or cisplatin damage in cells expressing WT, F112C or R130I XPA. Addition of either M113I or D114Y XPA to the reaction led to a notable but not statistically significant decrease of ∼25% of excision product accumulation compared to WT XPA (Figure 2A, B). We note that this effect is somewhat reduced relative to that observed in the survival assays (Figure 1A), which we attribute to the limitations of an *in vitro* reconstitution biochemical assay relative to

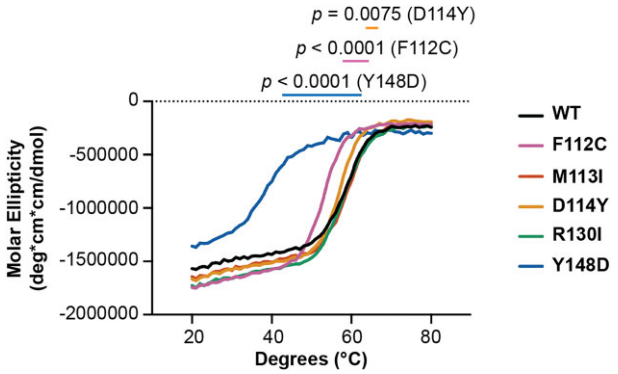

Figure 3. The Y148D variant destabilizes XPA. Circular dichroism of purified recombinant WT or variant XPA DBD protein measured at 222 nm over increasing temperature ($n = 3$). Each curve represents the average of three measurements. Ellipticities for the buffer and cuvette alone were subtracted from each measurement. Mean apparent T_m and standard deviation determined for each variant by recording the temperature at which the steepest slope is observed (the temperature at the maximum recorded value of the corresponding first derivative curve): 59 ± 0.6°C (WT), 53 ± 0.0°C (F112C), 59 ± 0.6°C (M113I), 57 ± 0.0°C (D114Y), 58 ± 1.0°C (R130I) and 38 ± 2.1°C (Y148D). Mean apparent T_m values were statistically compared for each variant to WT using two-tailed unpaired *t*-tests, and comparisons to WT with $P < 0.05$ are indicated.

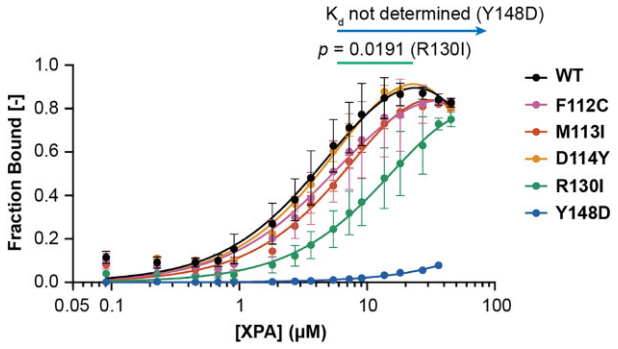

Figure 4. XPA tumor variants have disrupted DNA binding affinity. Microscale thermophoresis using a 5′ 6-FAM labeled hairpin DNA substrate with eight nucleotides (nt) of dsDNA and 4 nt of ssDNA overhang and indicated WT or variant purified recombinant XPA DBD (residues 98–239) protein performed at 20°C ($n = 5$ for WT, $n = 3$ for all variants). K_d values for the DNA substrate in each replicate were determined using lines of best fit from nonlinear regression analysis in GraphPad Prism (one site – total binding model). Error bars indicate the standard deviation. The mean and standard deviation K_d values were 7.7 ± 3.7 μM (WT), 9.2 ± 2.2 μM (F112C), 12 ± 1.9 μM (M113I), 8.8 ± 1.7 μM (D114Y), 38 ± 22 μM (R130I) and not determined (Y148D). Mean K_d values were statistically compared for each variant to WT using two-tailed unpaired t-tests, and comparisons to WT with $P < 0.05$ are indicated.

the cellular context. In the case of the Y148D variant, a much larger ∼50% decrease of excision product accumulation by the final 45-min timepoint (Figure 2A, B) was observed, independent of the decrease in protein seen in cells. These results suggest that the Y148D XPA variant leads to a functional protein defect in addition to increased cellular degradation. To obtain deeper insights, we set out to determine the mechanisms of NER dysfunction for these tumor variants by searching for evidence of perturbation of protein structure and stability, decreased DNA binding affinity, loss of protein–protein interaction and disruption of recruitment to sites of damage.

The Y148D mutation destabilizes XPA

A fundamental step in defining the molecular mechanisms of dysfunction for a variant is to determine if the mutation has any effect on the structural stability of the protein. To this end, we turned to circular dichroism (CD) spectroscopy to characterize the distribution and stability of secondary structural elements for the XPA variants. The previously well-characterized XPA DNA binding domain (DBD, $XPA_{98–239}$) was used for these experiments because it is the only part of the XPA that folds into a globular domain with regular secondary structure and all the variants investigated are within this domain. XPA DBD consists primarily of α-helical elements, (36,47–49) a characteristic that is well reflected in the CD data (Supplementary Figure S5), which show that all five variants retain the structure of the WT protein. The effect of the mutations on the thermal stability of XPA DBD was then assayed by measuring the thermal denaturation midpoint (T_m) derived from the temperature dependence of the CD spectra. Compared to WT, the M113I and R130I mutations had no effect on T_m (59 ± 0.6°C, 59 ± 0.6°C and 58 ± 1.0°C for WT, M113I and R130I, respectively), whereas F112C and D114Y had statistically significant but very modest decreases in T_m (53 ± 0.0°C and 57 ± 0.0°C for F112C and D114Y, respectively) (Figure 3). The T_m decrease of only a few degrees for either F112C or D114Y is highly unlikely to cause significant defects in the context of NER function. In contrast, the Y148D variant was dramatically destabilized (T_m 38 ± 2.1°C) to the extent that a significant population of the protein will be unfolded in cells, consistent with our observations of lower levels and degradation by the UPS in cells.

XPA tumor variants have disrupted DNA binding affinity

The binding of DNA by XPA is central to its function as a scaffold in NER, so the DNA binding affinity was measured for each XPA variant and compared to WT protein. Microscale thermophoresis (MST) with XPA DBD and a fluorescently labeled NER junction mimic substrate was used for these measurements. (32) The DNA binding affinity observed for WT DBD was comparable to that reported previously ($K_d = 7.7 \pm 3.7$ μM). (16,32,50) Among the five XPA variants, there was no effect on DNA binding affinity for F112C, M113I and D114Y (Figure 4), although this was perhaps expected because these residues do not contact DNA and instead are located within the RPA interaction interface on XPA. For R130I, a residue known to contact the DNA substrate, (32) we observed a statistically significant but very modest reduction in affinity ($K_d = 38 \pm 22$ μM). The small size of the effect reflects the limited contribution of any single residue within the large DNA binding surface on XPA, and is consistent with the lack of hypersensitivity to the UV and cisplatin. In contrast to the other variants, Y148D did not have any measurable affinity for DNA (Figure 4), suggesting the observed NER deficiency for this variant arises from a scaffolding defect in NER.

NER-deficient variants M113I and D114Y do not significantly disrupt interaction with RPA

We have shown previously that NER function requires interaction between XPA and RPA and that mutations within the RPA interaction interface of XPA can inhibit NER. (16,32) In the effort to discern the mechanistic basis for the NER defi-

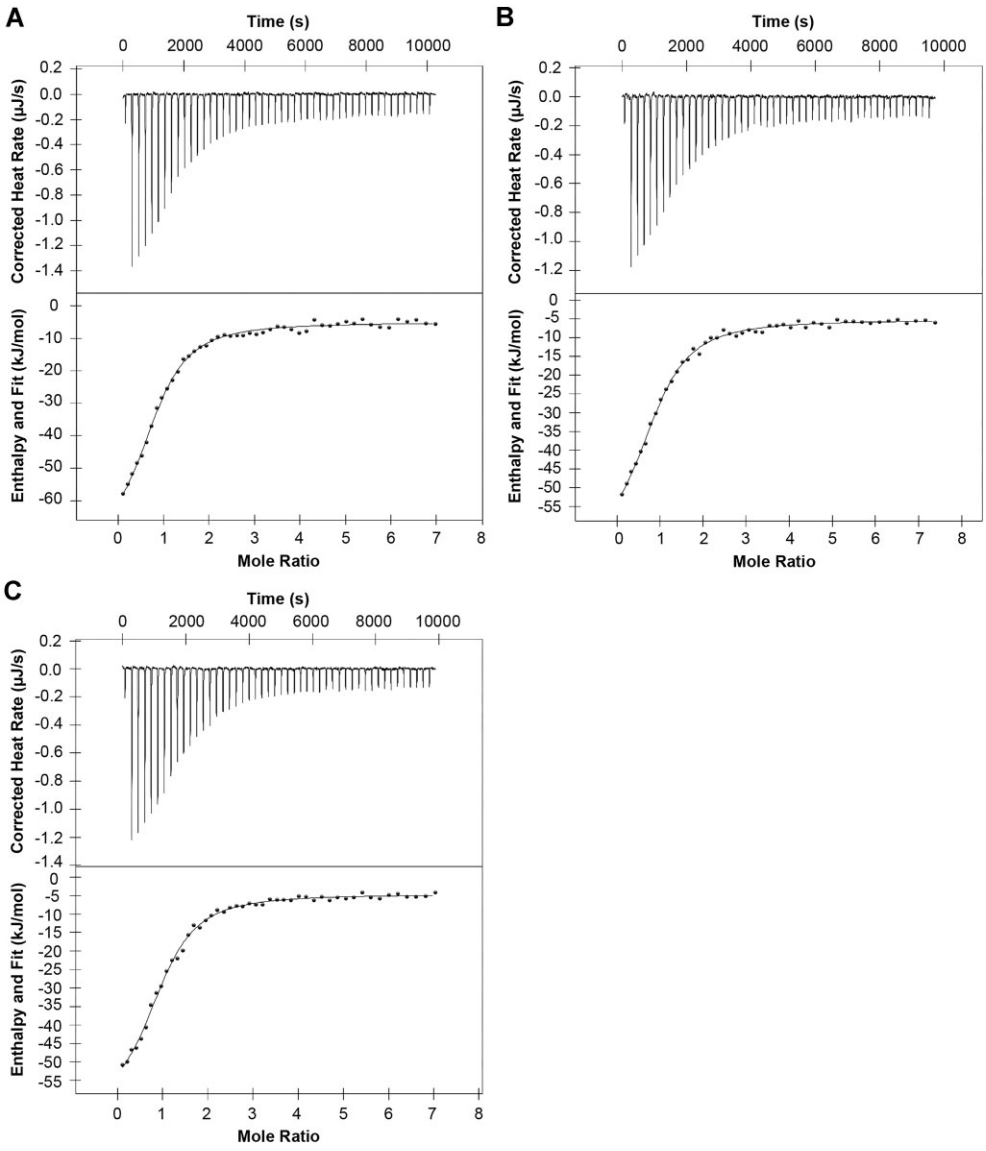

Figure 5. Single NER-deficient XPA variants M113I and D114Y do not significantly disrupt the essential scaffolding interaction with RPA. Isothermal titration calorimetry of purified recombinant full-length WT XPA ($n = 2$, **A**), M113I XPA ($n = 3$, **B**), and D114Y XPA ($n = 2$, **C**) and RPA. Representative thermograms showing the raw heat release (upper) and integrated heat release (lower) for each. The first injection of 0.5 μl was removed from each titration for analysis. The mean and standard deviation K_d values were 2.8 ± 1.7 μM (WT), 5.3 ± 1.1 μM (M113I), and 4.5 ± 4.9 μM (D114Y). Mean K_d values were statistically compared for each variant to WT using two-tailed unpaired *t*-tests: M113I $P = 0.2118$ and D114Y $P = 0.4161$.

ciencies observed for three of our variants (M113I, D114Y and Y148D), we set out to apply our isothermal titration calorimetry (ITC) approach to test the interaction of XPA with RPA. Attempts to apply this assay to Y148D were stymied by its limited solubility, which prevented concentrating the protein to a sufficiently high level for ITC analysis. The K_d values for M113I (5.3 ± 1.1 μM) and D114Y (4.5 ± 4.9 μM) were within the experimental error of the value for WT XPA (2.8 ± 1.7 μM) (Figure 5, Table 1). These results are consistent with our previous findings, which showed that single mutations within the interaction interface of the XPA DBD are insufficient to disrupt the XPA-RPA scaffold. (16,32)

Table 1. Thermodynamic parameters for the binding of XPA to RPA

XPA protein	K_d (μM)	n	ΔH (kJ/mol)	$-T\Delta S$ (kJ/mol)
WT	2.8 ± 1.7	1.0 ± 0.1	-56 ± 12	23.2 ± 13.7
M113I	5.3 ± 1.1	1.2 ± 0.2	-57 ± 3.4	26.4 ± 3.6
D114Y	4.5 ± 4.9	1.0 ± 0.0	-56 ± 1.2	25.5 ± 0.9

Recruitment to sites of UV damage and rate of repair is hindered for Y148D XPA tumor variant

As a NER scaffold protein, XPA interacts with many other NER factors as well as RPA and the DNA near a lesion, all of which are required to assemble the catalytically competent incision complex (51). Therefore, recruitment of XPA to the damaged site is integral to successful repair. The hypersensitivity of cells expressing M113I, D114Y or Y148D XPA to UV and cisplatin suggests a potential recruitment defect for these variants. To assess the recruitment of each XPA protein to sites of UV damage in cells, we used local UV irradiation and immunofluorescence to detect localization of each of the five

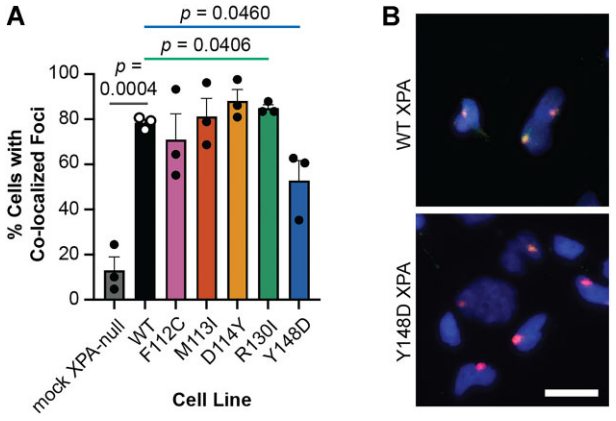

Figure 6. Recruitment to sites of UV damage is hindered for Y148D XPA tumor variant. (**A**) Local UV irradiation and immunofluorescence assay in stable XP2OS cell lines ($n = 3$). Cells were exposed to 120 J/m^2 UV irradiation through polycarbonate isopore membranes with 5 μm pores and XPA and 6–4PP damage foci were detected using immunofluorescence after 30 min incubation. XPA co-localization in at least 100 cells with 6–4PP foci was quantified per cell line using FIJI. Mean percent cells with co-localized foci were statistically compared in each variant-expressing cell line to WT using two-tailed unpaired *t*-tests, and comparisons to WT with $P < 0.05$ are indicated. (**B**) Representative merged images of local UV irradiation and immunofluorescence assay in stable XP2OS cell lines from (A). DAPI in blue, 6–4PP in red, XPA in green, strong co-localization in yellow. Scale bar 20 μm.

XPA variants to pyrimidine-pyrimidone (6–4) photoproducts (6–4PPs) that are classically repaired by NER (52). Among the five variants tested, only cells expressing Y148D XPA had a statistically significant decrease in XPA recruitment to 6–4PP damage sites compared to cells expressing WT XPA (Figure 6A, B, Supplementary Figure S6). This result agrees with the decreased DNA binding affinity observed for Y148D XPA, as well as a significantly slower rate of 6–4PP repair in cells expressing Y148D XPA (Supplementary Figure S7). Overall, the partial loss of recruitment for Y148D further confirms that a protein scaffolding defect in cells contributes to the NER deficiency for this variant.

Discussion

The observed correlation between defects in NER genes *ERCC1* and *ERCC2* and improved outcomes for patients treated with standard-of-care Pt agents suggests that information on the status of NER genes in tumors can be used to direct patient treatments. In this study, the novel tumor variants F112C, M113I, D114Y, R130I and Y148D were selected to test the correlation between sensitivity to UV and cisplatin induced DNA damage and elucidate mechanisms of variant dysfunction. These variants were identified by our previous work on predicting NER-deficient variants in XPA using machine learning (11).

The NER activity of each variant was first assessed in cells with UV lesions on native chromatin (Figure 1A) rather than the FM-HCR reporter plasmid used in our previous study. These analyses confirmed the previous FM-HCR results that only three of the five variants of interest displayed mild (M113I and D114Y) to moderate (Y148D) sensitivity to UV in cells. Due to the preliminary nature of the machine learning predictions that identified all five variants as NER-deficient, the failure to accurately predict the F112C and R130I variants as NER-*pro*ficient was not surprising. Interestingly, only cells expressing the Y148D variant with moderate sensitivity to UV were also more sensitive to cisplatin (Figure 1B). This lack of agreement was somewhat unexpected based on analyses of ERCC2 variants showing near perfect correlation between UV and cisplatin sensitivity. (6) However, cisplatin lesions are known to be repaired by additional pathways in cells including DSB repair and ICL repair (42) or overcome through translesion synthesis (TLS) (53). Compensation by other pathways may have masked the mild NER-specific sensitivities to cisplatin in cells, a hypothesis supported by the *in vitro* dual-incision assay, which revealed reproducible but not statistically significant reductions in excision of a NER-specific cisplatin lesion for the M113I and D114Y variants (Figure 2). A similar phenomenon has been observed in ERCC1-XPA interaction mutants, where disruption of interaction with ERCC1 dramatically sensitizes cells to UV, but not cisplatin (23). Although further investigation is necessary to better understand this discrepancy, including analysis of variants with more severe UV sensitivity, assays performed in cells deficient for DSB repair, ICL repair, or TLS, and quantification of genomic cisplatin-DNA damage using ICP-MS, these findings demonstrate that XPA tumor variants such as Y148D can predictably sensitize cells to cisplatin.

To better understand how the selected XPA tumor variants led to defective NER and increased cellular sensitivity to UV or cisplatin exposure, we investigated the potential mechanisms for dysfunction of each variant. While all five of the tumor variants studied here are located in the XPA DBD and were predicted to have defective NER, increased sensitivity to UV or cisplatin was only observed for three of the variants. This highlights the importance of performing functional analyses to better understand and overcome the limitations of the initial predictive machine learning framework. Moreover, our studies to identify mechanisms of dysfunction for the remaining variants yielded important insights into essential aspects of XPA function during NER. For example, the M113I and D114Y variants, which are positioned at the XPA interaction interface with RPA, exhibited only a mild increase in UV and cisplatin sensitivity but no detectable loss in RPA binding affinity despite their location within the RPA70AB interaction interface. Both of these observations are consistent with our previous work on the interaction between the XPA DBD and RPA70AB, which revealed that single-site mutations have only a mild effect on NER activity and that multiple mutations are needed to completely abrogate this interaction (16,32). The results obtained for the Y148D variant were more striking.

Y148D was the only variant assayed that increased cellular sensitivity to both UV and cisplatin, and a severe protein stability defect was identified (Figure 3), as well as disrupted DNA binding (Figure 4) and hindered protein recruitment to sites of UV damage in cells (Figure 6). Considering that the Y148D variant resulted in a change from a buried hydrophobic tyrosine residue to a negatively charged aspartic acid, the resulting loss of stability reflected by the 20°C reduction in T_m to 38°C is not surprising. For the isolated protein this thermodynamic instability translates to approximately half of the protein being unfolded in a living cell. The Y148D gene was expressed in cells at the same level as the WT protein, but less protein was observed in cells due at least in part to turnover by the UPS, which is consistent with the protein folding defect of the variant. The DNA binding affinity measurements performed at 20°C, a temperature

much lower than the T_m of Y148D where the equilibrium population of unfolded protein will be substantially lower, suggest that the loss of DNA binding affinity observed is a distinct phenotype and not solely the result of protein destabilization. This conclusion is also supported by the *in vitro* incision analyses comparing equal amounts of different XPA WT and variant proteins, which indicate that the hypersensitivity phenotype is not solely due to the decreased levels of Y148D XPA protein in cells. While Y148D XPA exhibited the most dramatic variant phenotype in our study, there were still statistically significant levels of NER activity in Y148D XPA-expressing cells compared to XPA-null cells (Figure 1 and Supplementary Figure S3), in agreement with previous study that even low levels of XPA can maintain NER activity (54). This finding highlights the broader importance of clinical studies including variants rather than solely knockout or knockdown models that may exaggerate phenotypes. The development of CRISPR/Cas9 XPA variant knock-in cell lines represents an important next step towards deeper understanding of the effects of mutations in the clinical setting.

The analyses performed did not exhaustively assay all possible mechanisms of dysfunction. Key areas of additional study will include assessing the downstream recruitment of additional NER factors to sites of damage and the XPA-RPA scaffold. Nevertheless, our results provide a sound basis for the observed defects in the Y148D variant cellular hypersensitivity to UV and cisplatin. In particular, protein destabilization and degradation were identified as key mechanisms of the Y148D variant dysfunction. These insights were obtained from combining both cell-based assays and biophysical and structural analyses; neither strategy alone can provide a full explanation of variant effect on the cell. Specifically, when considering the non-enzymatic scaffolding role that XPA plays during NER, these results emphasize the importance of including protein stability metrics in future variant effect prediction efforts. More broadly, these data suggest that the predictive power of the preexisting machine learning framework can be improved by ensuring that the input training data includes metrics that reflect deleterious mechanisms known to reduce NER and sensitize cells to cisplatin as well as UV. Combined with further exploration of sensitivity to other commonly used Pt drugs such as carboplatin and oxaliplatin (55) and characterization of variants with more severe NER defects, these studies have the potential to dramatically improve XPA variant effect prediction.

Taken together, the characterization of selected XPA tumor variants predicted to sensitize cells to cisplatin revealed that XPA protein stability and scaffold function are essential for NER and that variant protein dysfunction or loss can sensitize cells to cisplatin. These findings suggest that deleterious XPA tumor variants should be considered when predicting patient response to Pt-based chemotherapeutics, in addition to variants in other NER genes such as *ERCC2* and in genes in other DNA repair pathways. Considering the relatively low somatic mutation frequency for *XPA*, identifying and characterizing sensitizing variants in additional genes and pathways is essential to fully understand the true impact of protein variants on chemotherapy response. The ability to accurately identify such variants and determine common mechanisms of dysfunction, such as destabilization and cellular degradation of XPA, remains essential for precision medicine approaches. Finally, these findings provide the foundation to test whether inclusion of mechanistic insights, such as measures of protein stability for XPA variant interpretation, significantly improve the accuracy of machine learning predictions.

Data availability

The data generated in this study are available within the article and its supplementary files. Unique reagents including plasmids generated are available upon request to the corresponding author.

Supplementary data

Supplementary Data are available at NAR Cancer Online.

Acknowledgements

We acknowledge Anais Naretto for her assistance handling the platinum reagents. The graphical abstract was created with a licensed version of BioRender.com.

Author contributions: Conceptualization: W.J.C., A.M.B.; Methodology: A.M.B., K.S.G., M.K., H.S.K., S.S.K., W.J.C.; Software: A.M.B.; Validation: A.M.B., K.S.G.; Formal Analysis: A.M.B., K.S.G., M.K., H.S.K., S.S.K., W.J.C.; Resources: O.D.S., A.M.B.; Investigation: A.M.B., K.S.G., M.K., H.S.K., S.S.K., C.R.T., A.D., A.N., P.D.N., J.P.; Data Curation: N/A; Writing – Original Draft: A.M.B., W.J.C.; Writing – Review and Editing: A.M.B., K.S.G., M.K., H.S.K., O.D.S., W.J.C.; Visualization: A.M.B., K.S.G., M.K., H.S.K., S.S.K.; Supervision: O.D.S., W.J.C.; Project Administration: N/A; Funding Acquisition: W.J.C., O.D.S., A.M.B.

Funding

NIH [F32 CA250258, P01 CA092584, R01 CA218315, T32 CA009582]; Korean Institute for Basic Science [IBS-R022-A1]; Vanderbilt-Ingram Cancer Center [P30CA068485].

Conflicts of interest statement

None declared.

References

1. Gillet,L.C. and Scharer,O.D. (2006) Molecular mechanisms of mammalian global genome nucleotide excision repair. *Chem. Rev.*, **106**, 253–276.
2. Marteijn,J.A., Lans,H., Vermeulen,W. and Hoeijmakers,J.H. (2014) Understanding nucleotide excision repair and its roles in cancer and ageing. *Nat. Rev. Mol. Cell Biol.*, **15**, 465–481.
3. Lehmann,A.R. (2003) DNA repair-deficient diseases, xeroderma pigmentosum, Cockayne syndrome and trichothiodystrophy. *Biochimie*, **85**, 1101–1111.
4. Kraemer,K.H., Patronas,N.J., Schiffmann,R., Brooks,B.P., Tamura,D. and DiGiovanna,J.J. (2007) Xeroderma pigmentosum, trichothiodystrophy and Cockayne syndrome: a complex genotype-phenotype relationship. *Neuroscience*, **145**, 1388–1396.
5. Arora,S., Kothandapani,A., Tillison,K., Kalman-Maltese,V. and Patrick,S.M. (2010) Downregulation of XPF-ERCC1 enhances cisplatin efficacy in cancer cells. *DNA Repair (Amst.)*, **9**, 745–753.
6. Li,Q., Damish,A.W., Frazier,Z., Liu,D., Reznichenko,E., Kamburov,A., Bell,A., Zhao,H., Jordan,E.J., Gao,S.P., *et al.* (2019) ERCC2 Helicase domain mutations confer nucleotide excision repair deficiency and drive cisplatin sensitivity in muscle-invasive bladder cancer. *Clin. Cancer Res.*, **25**, 977–988.

7. Liu,D., Plimack,E.R., Hoffman-Censits,J., Garraway,L.A., Bellmunt,J., Van Allen,E. and Rosenberg,J.E. (2016) Clinical validation of chemotherapy response biomarker ERCC2 in muscle-invasive urothelial bladder carcinoma. *JAMA Oncol.*, **2**, 1094–1096.
8. Van Allen,E.M., Mouw,K.W., Kim,P., Iyer,G., Wagle,N., Al-Ahmadie,H., Zhu,C., Ostrovnaya,I., Kryukov,G.V., O'Connor,K.W., *et al.* (2014) Somatic ERCC2 mutations correlate with cisplatin sensitivity in muscle-invasive urothelial carcinoma. *Cancer Discov.*, **4**, 1140–1153.
9. Knijnenburg,T.A., Wang,L., Zimmermann,M.T., Chambwe,N., Gao,G.F., Cherniack,A.D., Fan,H., Shen,H., Way,G.P., Greene,C.S., *et al.* (2018) Genomic and molecular landscape of DNA damage repair deficiency across the cancer genome atlas. *Cell Rep.*, **23**, 239–254.
10. Green,E.D., Gunter,C., Biesecker,L.G., Di Francesco,V., Easter,C.L., Feingold,E.A., Felsenfeld,A.L., Kaufman,D.J., Ostrander,E.A., Pavan,W.J., *et al.* (2020) Strategic vision for improving human health at the forefront of genomics. *Nature*, **586**, 683–692.
11. Blee,A.M., Li,B., Pecen,T., Meiler,J., Nagel,Z.D., Capra,J.A. and Chazin,W.J. (2022) An active learning framework improves tumor variant interpretation. *Cancer Res.*, **82**, 2704–2715.
12. Cerami,E., Gao,J., Dogrusoz,U., Gross,B.E., Sumer,S.O., Aksoy,B.A., Jacobsen,A., Byrne,C.J., Heuer,M.L., Larsson,E., *et al.* (2012) The cBio cancer genomics portal: an open platform for exploring multidimensional cancer genomics data. *Cancer Discov.*, **2**, 401–404.
13. de Bruijn,I., Kundra,R., Mastrogiacomo,B., Tran,T.N., Sikina,L., Mazor,T., Li,X., Ochoa,A., Zhao,G., Lai,B., *et al.* (2023) Analysis and visualization of longitudinal genomic and clinical data from the AACR Project GENIE Biopharma Collaborative in cBioPortal. *Cancer Res.*, **83**, 3861–3867.
14. Gao,J., Aksoy,B.A., Dogrusoz,U., Dresdner,G., Gross,B., Sumer,S.O., Sun,Y., Jacobsen,A., Sinha,R., Larsson,E., *et al.* (2013) Integrative analysis of complex cancer genomics and clinical profiles using the cBioPortal. *Sci. Signal*, **6**, pl1.
15. Takebe,H., Nii,S., Ishii,M.I. and Utsumi,H. (1974) Comparative studies of host-cell reactivation, colony forming ability and excision repair after UV irradiation of xeroderma pigmentosum, normal human and some other mammalian cells. *Mutat. Res.*, **25**, 383–390.
16. Kim,M., Kim,H.S., D'Souza,A., Gallagher,K., Jeong,E., Topolska-Wos,A., Meur,O.L., K.,T., C.L.,T., M.S.,K., *et al.*2022) Two interaction surfaces between XPA and RPA organize the preincision complex in nucleotide excision repair. *Proc. Nat. Acad. Sci. U.S.A.*, **119**, e2207408119.
17. Cheon,N.Y., Kim,H.S., Yeo,J.E., Scharer,O.D. and Lee,J.Y. (2019) Single-molecule visualization reveals the damage search mechanism for the human NER protein XPC-RAD23B. *Nucleic Acids Res.*, **47**, 8337–8347.
18. Hohl,M., Thorel,F., Clarkson,S.G. and Scharer,O.D. (2003) Structural determinants for substrate binding and catalysis by the structure-specific endonuclease XPG. *J. Biol. Chem.*, **278**, 19500–19508.
19. Enzlin,J.H. and Scharer,O.D. (2002) The active site of the DNA repair endonuclease XPF-ERCC1 forms a highly conserved nuclease motif. *EMBO J.*, **21**, 2045–2053.
20. Gradia,S.D., Ishida,J.P., Tsai,M.S., Jeans,C., Tainer,J.A. and Fuss,J.O. (2017) MacroBac: new technologies for robust and efficient large-scale production of recombinant multiprotein complexes. *Methods Enzymol.*, **592**, 1–26.
21. Pfaffl,M.W. (2001) A new mathematical model for relative quantification in real-time RT-PCR. *Nucleic Acids Res.*, **29**, e45.
22. Franken,N.A., Rodermond,H.M., Stap,J., Haveman,J. and van Bree,C. (2006) Clonogenic assay of cells in vitro. *Nat. Protoc.*, **1**, 2315–2319.
23. Orelli,B., McClendon,T.B., Tsodikov,O.V., Ellenberger,T., Niedernhofer,L.J. and Scharer,O.D. (2010) The XPA-binding domain of ERCC1 is required for nucleotide excision repair but not other DNA repair pathways. *J. Biol. Chem.*, **285**, 3705–3712.
24. Rafehi,H., Orlowski,C., Georgiadis,G.T., Ververis,K., El-Osta,A. and Karagiannis,T.C. (2011) Clonogenic assay: adherent cells. *J. Vis. Exp.*, **49**, 2573.
25. Orellana,E.A. and Kasinski,A.L. (2016) Sulforhodamine B (SRB) assay in cell culture to investigate cell proliferation. *Biol. Protoc.*, **6**, e1984.
26. Vichai,V. and Kirtikara,K. (2006) Sulforhodamine B colorimetric assay for cytotoxicity screening. *Nat. Protoc.*, **1**, 1112–1116.
27. Voigt,W. (2005) Sulforhodamine B assay and chemosensitivity. *Methods Mol. Med.*, **110**, 39–48.
28. Kolbanovskiy,M., Aharonoff,A., Sales,A.H., Geacintov,N.E. and Shafirovich,V. (2020) Remarkable enhancement of nucleotide excision repair of a bulky guanine lesion in a covalently closed circular DNA plasmid relative to the same linearized plasmid. *Biochemistry*, **59**, 2842–2848.
29. Greenfield,N.J. (2006) Using circular dichroism spectra to estimate protein secondary structure. *Nat. Protoc.*, **1**, 2876–2890.
30. Holt,M.E., Salay,L.E. and Chazin,W.J. (2017) A polymerase with potential: the Fe-S cluster in Human DNA primase. *Methods Enzymol.*, **595**, 361–390.
31. Salay,L.E., Blee,A.M., Raza,M.K., Gallagher,K.S., Chen,H., Dorfeuille,A.J., Barton,J.K. and Chazin,W.J. (2022) Modification of the 4Fe-4S cluster charge transport pathway alters RNA synthesis by yeast DNA primase. *Biochemistry*, **61**, 1113–1123.
32. Topolska-Wos,A.M., Sugitani,N., Cordoba,J.J., Le Meur,K.V., Le Meur,R.A., Kim,H.S., Yeo,J.E., Rosenberg,D., Hammel,M., Scharer,O.D., *et al.* (2020) A key interaction with RPA orients XPA in NER complexes. *Nucleic Acids Res.*, **48**, 2173–2188.
33. Volker,M., Mone,M.J., Karmakar,P., van Hoffen,A., Schul,W., Vermeulen,W., Hoeijmakers,J.H., van Driel,R., van Zeeland,A.A. and Mullenders,L.H. (2001) Sequential assembly of the nucleotide excision repair factors in vivo. *Mol. Cell*, **8**, 213–224.
34. Buchko,G.W., Daughdrill,G.W., de Lorimier,R., Rao,B.K., Isern,N.G., Lingbeck,J.M., Taylor,J.S., Wold,M.S., Gochin,M., Spicer,L.D., *et al.* (1999) Interactions of human nucleotide excision repair protein XPA with DNA and RPA70 delta C327: chemical shift mapping and 15N NMR relaxation studies. *Biochemistry*, **38**, 15116–15128.
35. Buchko,G.W., Ni,S., Thrall,B.D. and Kennedy,M.A. (1998) Structural features of the minimal DNA binding domain (M98-F219) of human nucleotide excision repair protein XPA. *Nucleic Acids Res.*, **26**, 2779–2788.
36. Ikegami,T., Kuraoka,I., Saijo,M., Kodo,N., Kyogoku,Y., Morikawa,K., Tanaka,K. and Shirakawa,M. (1998) Solution structure of the DNA- and RPA-binding domain of the human repair factor XPA. *Nat. Struct. Biol.*, **5**, 701–706.
37. Lian,F.M., Yang,X., Yang,W., Jiang,Y.L. and Qian,C. (2019) Structural characterization of the redefined DNA-binding domain of human XPA. *Biochem. Biophys. Res. Commun.*, **514**, 985–990.
38. Myung,J., Kim,K.B. and Crews,C.M. (2001) The ubiquitin-proteasome pathway and proteasome inhibitors. *Med. Res. Rev.*, **21**, 245–273.
39. Park,J., Cho,J. and Song,E.J. (2020) Ubiquitin-proteasome system (UPS) as a target for anticancer treatment. *Arch Pharm Res*, **43**, 1144–1161.
40. Adzhubei,I.A., Schmidt,S., Peshkin,L., Ramensky,V.E., Gerasimova,A., Bork,P., Kondrashov,A.S. and Sunyaev,S.R. (2010) A method and server for predicting damaging missense mutations. *Nat. Methods*, **7**, 248–249.
41. Adams,J., Behnke,M., Chen,S., Cruickshank,A.A., Dick,L.R., Grenier,L., Klunder,J.M., Ma,Y.T., Plamondon,L. and Stein,R.L. (1998) Potent and selective inhibitors of the proteasome: dipeptidyl boronic acids. *Bioorg. Med. Chem. Lett.*, **8**, 333–338.
42. Rocha,C.R.R., Silva,M.M., Quinet,A., Cabral-Neto,J.B. and Menck,C.F.M. (2018) DNA repair pathways and cisplatin resistance: an intimate relationship. *Clinics (Sao Paulo)*, **73**, e478s.

43. Huang,J.C., Zamble,D.B., Reardon,J.T., Lippard,S.J. and Sancar,A. (1994) HMG-domain proteins specifically inhibit the repair of the major DNA adduct of the anticancer drug cisplatin by human excision nuclease. *Proc. Nat. Acad. Sci. U.S.A.*, **91**, 10394–10398.
44. Moggs,J.G., Szymkowski,D.E., Yamada,M., Karran,P. and Wood,R.D. (1997) Differential human nucleotide excision repair of paired and mispaired cisplatin-DNA adducts. *Nucleic Acids Res.*, **25**, 480–491.
45. Moggs,J.G., Yarema,K.J., Essigmann,J.M. and Wood,R.D. (1996) Analysis of incision sites produced by human cell extracts and purified proteins during nucleotide excision repair of a 1,3-intrastrand d(GpTpG)-cisplatin adduct. *J. Biol. Chem.*, **271**, 7177–7186.
46. Zamble,D.B., Mu,D., Reardon,J.T., Sancar,A. and Lippard,S.J. (1996) Repair of cisplatin–DNA adducts by the mammalian excision nuclease. *Biochemistry*, **35**, 10004–10013.
47. Li,L., Lu,X., Peterson,C.A. and Legerski,R.J. (1995) An interaction between the DNA repair factor XPA and replication protein A appears essential for nucleotide excision repair. *Mol. Cell. Biol.*, **15**, 5396–5402.
48. Lian,F.M., Yang,X., Jiang,Y.L., Yang,F., Li,C., Yang,W. and Qian,C. (2020) New structural insights into the recognition of undamaged splayed-arm DNA with a single pair of non-complementary nucleotides by human nucleotide excision repair protein XPA. *Int. J. Biol. Macromol.*, **148**, 466–474.
49. Lian,F.M., Yang,X., Yang,W., Jiang,Y.L. and Qian,C. (2019) The redefined DNA-binding domain of human xeroderma pigmentosum complementation group A: production, crystallization and structure solution. *Acta Crystallogr. F Struct. Biol. Commun.*, **75**, 62–66.
50. Sugitani,N., Voehler,M.W., Roh,M.S., Topolska-Wos,A.M. and Chazin,W.J. (2017) Analysis of DNA binding by human factor xeroderma pigmentosum complementation group A (XPA) provides insight into its interactions with nucleotide excision repair substrates. *J. Biol. Chem.*, **292**, 16847–16857.
51. D'Souza,A., Blee,A.M. and Chazin,W.J. (2022) Mechanism of action of nucleotide excision repair machinery. *Biochem. Soc. Trans.*, **50**, 375–386.
52. Scharer,O.D. (2013) Nucleotide excision repair in eukaryotes. *Cold Spring Harb. Perspect. Biol.*, **5**, a012609.
53. Yamanaka,K., Chatterjee,N., Hemann,M.T. and Walker,G.C. (2017) Inhibition of mutagenic translesion synthesis: a possible strategy for improving chemotherapy?*PLoS Genet.*, **13**, e1006842.
54. Muotri,A.R., Marchetto,M.C., Suzuki,M.F., Okazaki,K., Lotfi,C.F., Brumatti,G., Amarante-Mendes,G.P. and Menck,C.F. (2002) Low amounts of the DNA repair XPA protein are sufficient to recover UV-resistance. *Carcinogenesis*, **23**, 1039–1046.
55. Rottenberg,S., Disler,C. and Perego,P. (2021) The rediscovery of platinum-based cancer therapy. *Nat. Rev. Cancer*, **21**, 37–50.

Received: August 11, 2023. **Revised:** January 27, 2024. **Editorial Decision:** February 26, 2024. **Accepted:** February 29, 2024